Available online at www.sciencedirect.com
SCIENCE DIRECT
Physics Letters A 355 (2006) 66–72
PHYSICS LETTERS A
www.elsevier.com/locate/pla

Electrical and thermal transport properties of the electron-doped manganites $La_{0.9-x}Y(Ho)_xTe_{0.1}MnO_3$

Gan-Hong Zheng, Yu-Ping Sun *, Xue-Bing Zhu, Wen-Hai Song

Key Laboratory of Materials Physics, Institute of Solid State Physics, Chinese Academy of Sciences, Hefei 230031, PR China

Received 18 October 2005; accepted 31 January 2006

Available online 13 February 2006

Communicated by J. Flouquet

Abstract

Systematical studies of resistivity $\rho(T)$, thermopower $S(T)$, and thermal conduction $\kappa(T)$ have been performed on the electron-doped manganites $La_{0.9-x}A_xTe_{0.1}MnO_3$ (A = Y or Ho, $0.05 \leqslant x \leqslant 0.15$). The Y005, Y010, Ho005 and Ho010 samples exhibit double insulator–metal (I–M) transitions in the $\rho(T)$ curves, one is very close to its Curie temperature T_C, the other is well below T_C. However, the Y015 and Ho015 samples present insulating behaviors in the whole measured temperature. S shows positive sign for all samples with a peak near T_C and a bump/peak in the ferromagnetic (FM) region. The $\rho(T)$ and $S(T)$ data above T_C can be fitted well by the variable-range hopping (VRH) model. The small thermal conduction data suggests that there exists a large JT distortion in the studied samples. Moreover, comparing with the Y-doped compounds, the Ho-doped ones have smaller the thermal conduction value. This result is discussed as the existence of antiferromagnetic (AFM) coupling between Ho and Mn ions in the Ho-doping samples. On the one hand, the magnetic disorder enhancement due to the competition of ferromagnetic (FM) and AFM lower the thermal conductivity, on the other hand, the AFM coupling will reduce the phonon–phonon scattering.

PACS: 75.47.Lx; 75.30.Hx; 75.50.Ee

Keywords: Manganites; Antiferromagnetic coupling; Thermopower; Heat conductivity

1. Introduction

The discovery of colossal magentoresistance (CMR) in the hole-doped manganites has been the subject of intense work for their possible applications such as magnetic reading heads, field sensors and memories [1–3]. Traditionally, the CMR phenomenon is explained by the double-exchange (DE) interaction between Mn^{3+} and Mn^{4+} ions [4]. In addition, the local Jahn–Teller (JT) distortion is also suggested to play a key role in these manganties [5]. Recently, electron-doped compounds in which Ln were substituted by tetravalent ion such as Ce^{4+}, Te^{4+} and Zr^{4+}, etc., have been studied by some research groups [6–8]. These studies indicated that CMR behavior could occur in the system of a mixed-valence state of Mn^{2+} and Mn^{3+}.

The electrical transports $\rho(T)$, thermopower $S(T)$ and thermal conductivity $\kappa(T)$ have been studied extensively for the hole-doped manganites [9–12], however, less attention has been focused on the electron-doped manganites [6]. In this work, we have investigated the electrical transports $\rho(T)$, thermopower $S(T)$, and thermal conductivity $\kappa(T)$ for the electron-doped manganites $La_{0.9-x}A_xTe_{0.1}MnO_3$ (A = Y or Ho, $0.05 \leqslant x \leqslant 0.15$). And the results show that the electronic conduction at high temperatures for all samples is followed by variable-range hopping (VRH) mechanism based on the fitting of the resistivity and thermopower data. The small thermal conduction suggests there exists large JT distortion in the studied samples. Moreover, comparing with the Y-doped manganites, the Ho-doped manganites have smaller the thermal conduction value. This result is discussed as the existence of antiferromagnetic (AFM) coupling between Ho and Mn ions in the Ho-doping samples. On the one hand, the magnetic disorder enhancement due to the competition of ferromagnetic

* Corresponding author. Tel.: +86 551 559 1436; fax: +86 551 559 1434.
E-mail address: ypsun@issp.ac.cn (Y.-P. Sun).

0375-9601/$ – see front matter
doi:10.1016/j.physleta.2006.01.095

(FM) and AFM lower the thermal conductivity, on the other hand, the AFM coupling will reduce the phonon–phonon scattering.

2. Experimental

Polycrystalline samples with nominal compositions $La_{0.9-x}A_xTe_{0.1}MnO_3$ where A = Y and Ho ($x = 0.05$, 0.10 and 0.15, which are referred to as Y005, Y010, Y015, Ho005, Ho010 and Ho015 below) were prepared by solid-state reaction method. Stoichiometric high-purity La_2O_3, Y_2O_3(Ho_2O_3), TeO_2 and MnO_2 powders were mixed and ground, and then heated in air at 750 °C for 24 h. The powder obtained was ground, pelletized, and sintered at 1100 °C for 24 h with three intermediate grinding, and finally, the furnace was cooled down to the room temperature. The structure and lattice constant were determined by powder X-ray diffraction using Cu K_a radiation at the room temperature. The resistance was measured by the standard four-probe method from 5 to 350 K. The thermopower and thermal conductivity were measured in a commercial physical property measurement system (PPMS, $1.8 \leqslant T \leqslant 400$ K, $0 \leqslant H \leqslant 9$ T) from 5 to 350 K.

3. Results and discussion

3.1. X-ray diffraction

Fig. 1(a) shows the XRD pattern of $La_{0.9-x}Y(Ho)_xTe_{0.1}MnO_3$ ($x = 0.05$, 0.10 and 0.15) samples. It can be found that all samples are single phase with no detectable secondary phases. XRD patterns for all samples can be indexed by rhombohedral lattice with the space group $R\bar{3}C$, and we present experimental and calculated XRD patterns for the Ho015 sample in Fig. 1(b). It can be seen that the fitting between the experimental spectra and calculated values is relatively good. The structural parameters are refined by the standard Rietveld technique and the fitting between the experimental spectra and the calculated values are shown in Table 1.

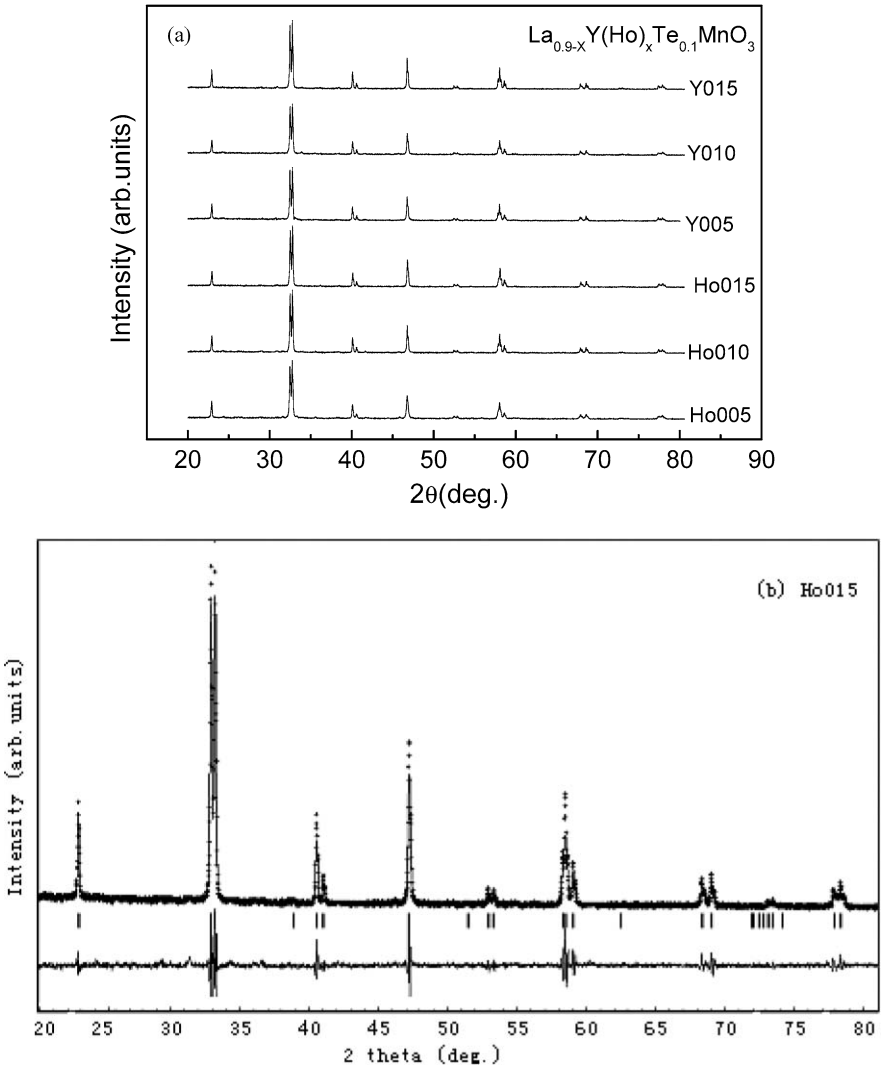

Fig. 1. (a) XRD patterns of the compound $La_{0.9-x}Y(Ho)_xTe_{0.1}MnO_3$ ($x = 0.05$, 0.10, 0.15). (b) The experimental and calculated XRD patterns of the compound Ho015. Crosses indicate the experimental data and the calculated data is continuous line overlapping them. The lowest curve shows the difference between experimental and calculated patterns. The vertical bars indicated the expected reflection positions.

Table 1
Structure parameters of $La_{0.9-x}Y(Ho)_xTe_{0.1}MnO_3$ ($x = 0.05$, 0.10, and 0.15) samples

Parameter	Y005	Y01	Y015	Ho005	Ho01	H0015
a (Å)	5.4855(20)	5.4866(18)	5.4881(21)	5.4798(20)	5.4901(18)	5.4908(21)
c (Å)	13.2658(32)	13.2664(13)	13.2680(27)	13.2752(31)	13.2799(25)	13.2728(25)
V (Å)^3	345.70	345.85	346.08	344.70	346.64	347.33
Mn–O (Å)	1.8502	1.8795	1.8825	1.8364	1.8924	1.9738
Mn–O–Mn (Å)	166.71	164.58	161.39	162.99	162.41	161.72
R_p (%)	9.55	10.99	10.23	11.90	9.89	10.03

From Table 1, it can be seen that the Mn–O–Mn bond angle decreases with increasing the doping level x for the same doping element, whereas the Mn–O bond length increases which displays the inverse correlation to the variation in the Mn–O–Mn bond angle. It is well known that there are two possible origins of the lattice distortion of the perovskite structures: one is the deformation of the MnO_6 octahedra originating from the JT effect which is decided by the concentration of Mn^{3+} ions, and the other is the average ionic radius of the A-site element $\langle r_A \rangle$. In the present samples, the concentration of Mn^{3+} is fixed for both Y-doping and Ho-doping samples and the lattice distortion is ascribed to the variation of the average A-site radius $\langle r_A \rangle$, induced by the substitution of smaller $Y(Ho)^{3+}$ for larger La^{3+} ions. Moreover, it can be seen that for the same doping level, there is nearly same lattice constant.

3.2. Resistivity

Fig. 2 shows the temperature dependence of resistivity $\rho(T)$ of both Y and Ho compounds in the temperature region of 5–350 K. For $x = 0.05$ composition, an insulator–metal (I–M) transition at $T_{P1} = 212$ and 206 K is observed for Y005 and Ho005 samples, respectively, which is very close their Curie temperature. In addition, there exist bump shoulders at 172 and 168 K (denoted by T_{P2}) in the FM phase region for Y005 and Ho005 samples, respectively, which is similar to the double peaks behavior observed in the alkaline-earth-metal-doped and alkali-metal-doped samples of $LaMnO_3$ [13–16]. As discussed in Ref. [18], T_{P1} is very close their Curie temperature T_C and it is related to ferromagnetic phase transition. In Ref. [18], T_{P2} is the second metal insulator transition temperature, which results from the competition of FM insulting (FMI) and FM metal (FMM). According to the DE model, in the homogeneous FM state, the electrons are mobile and the FM state and metallic state should accompany and facilitate each other. In contrast, the transport property of the now studied samples does not fully show metallic state below T_C. This FMI is also found in recent intensive studies [7–9]. The FM order at low temperatures for the studied samples can be regarded as FM clusters. On the one hand, based on the coexistence of FM clusters and AFM insulating phase in the low temperature region, we may suggest that the spatially inhomogeneous metallic and insulating areas coexist in the studied samples. When the system is transferred from paramagnetic (PM) to FM phase with the decrease of temperatures, the transport properties of these samples do not fully show the metallic state because the FMM phases are disconnected for the existence of the FMI phases

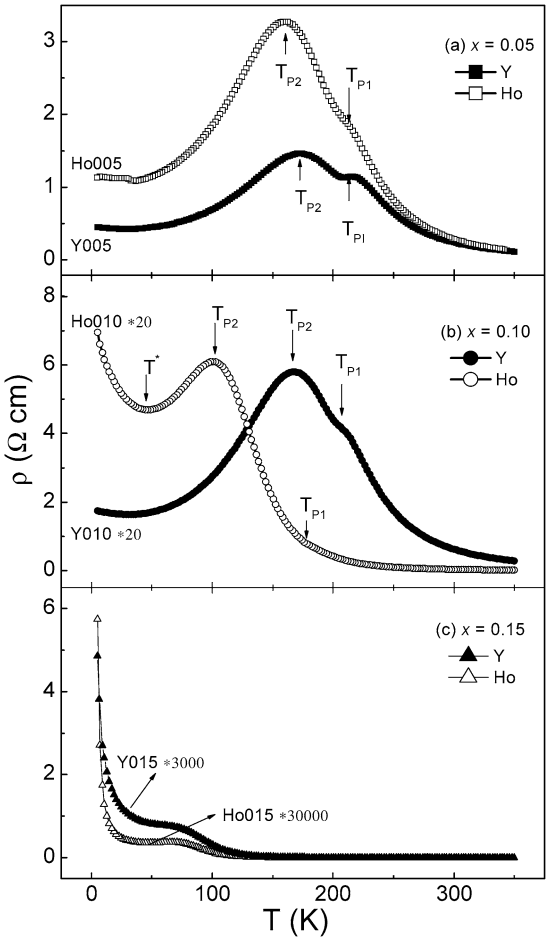

Fig. 2. The temperature dependence of the resistivity $\rho(T)$ of $La_{0.9-x}Y(Ho)_xTe_{0.1}MnO_3$ with (a) $x = 0.05$, (b) $x = 0.10$, and (c) $x = 0.15$.

among them. Fig. 2(b) shows $\rho(T)$ behavior for $x = 0.10$ composition. Compared with the Y005 sample, double peaks for the Y010 sample shift to lower temperatures, i.e., $T_{P1} = 206$ and $T_{P2} = 168$ K. For the Ho010 sample, the I–M transition at T_{P1} (= 183 K) is almost invisible and the I–M transition at T_{P2} (= 100 K) becomes more obvious. In other words, Y and Ho doping at A-site can substantially enhance the I–M transition at T_{P2} and suppress the I–M transition at T_{P1}. Moreover, for the Ho010 sample, an upturn of $\rho(T)$ behavior can be observed in the low temperature region, which is a smooth transition into a state with localized charge carriers on decreasing temperatures, as observed in many disordered materials. The $\rho(T)$ behavior is somewhat similar to what have been reported for the hole-doped $(La_{0.786}Y_{0.214})_{0.7}Ca_{0.3}MnO_3$ and

Table 2
Electrical and thermal parameters of $La_{0.9-x}Y(Ho)_xTe_{0.1}MnO_3$ ($x = 0.05$, 0.10, and 0.15) samples

Parameter	Y005	Y010	Y015	Ho005	Ho010	Ho015
T_C (K)	212	208	168	210	185	158
T_{P1} (K)	212	206	165	208	183	156
T_{P2} (K)	172	168	78	153	100	65
T^* (K)	–	–	45	–	44	38
$T_0(\times 10^7)$ (K)	5.67	6.66	10.55	7.74	8.67	12.14
T_{S1} (K)	235	224	176	235	214	174
T_{S2} (K)	122	115	90	122	115	100
$T\kappa$ (K)	212	209	–	212	–	–

$(La_{0.757}Dy_{0.243})_{0.7}Ca_{0.3}MnO_3$ manganites [17]. When the doping level x is increased to 0.15, the peak at T_{P1} and the bump at T_{P2} are all suppressed for the Y015 and Ho015 samples and the curves $\rho(T)$ seem as semiconducting behaviors. T_{P1} and T_{P2} are listed in Table 2. In addition, we can see that the resistivity ρ increases with increasing doping level for both Y and Ho compounds. The phenomenon is usually explained according to decreased average ionic radius of the A-site element $\langle r_A \rangle$ with increasing doping level x, which weakens the FM coupling due to the reduced band width of e_g electron. Moreover, the resistivity ρ of the Ho-doped compounds is larger than that of the Y-doped ones for the same doping level, which is attributed to the existence of AFM coupling between the magnetic moment of Ho and that of Mn ions for the Ho-doped samples as discussed in Ref. [18]. The similar phenomenon has been reported in $La_{1-x}Gd_xMnO_3$ and $Ga_{0.67}Ca_{0.33}MnO_3$ [19,20].

In order to investigate the electronic transport properties further, we use the small polaron (SP) hopping $\rho = BT\exp(E_a/k_BT)$ and VRH $\rho \sim \exp(T_0/T)^{1/4}$ [21] to fit the resistivity data. The fitting results as plotted in Fig. 3(a) and (b) indicate that the $\rho(T)$ data above T_{P1} for all samples can be well described by the VRH model with the fitting parameter T_0. The fitting parameter T_0, as summarized in Table 2, is related to the localization length ξ by the expression $k_BT_0 \approx 21/[\xi^3 N(E_F)]$, where k_B is Boltzman constant, $N(E_F)$ is the electronic density of states in the vicinity of the Fermi energy level. Since Y or Ho-doping does not change the Mn^{2+}/Mn^{3+} ratio, it is reasonable to assume the $N(E_F)$ is nearly independent on the doping level and element. Therefore, the variation of T_0 with the doping level reflects the change of localization length. From Table 2, it can be seen that the T_0 value increases obviously with an increase of the doping level x for the same doping element, implying the decrease of the localization length and the reduction of the carrier mobility. For the same composition, the larger value of T_0 of the Ho-doped compounds compared with that of Y-doped ones implies the smaller localization length and the weaker carrier mobility, which is intimately related to the localization of carriers and the variation of DE interaction. It suggested further that there exists AFM coupling in the Ho-doping samples.

Based on the above discussion, the conduction above T_{P1} may be governed by the VRH mechanism in the studied samples. And the fitting results obtained indicate that smaller localization length and the weaker carrier mobility in the Ho-doping samples due to the existence of AFM coupling in between Ho and Mn ions. The following analysis of the thermopower $S(T)$ fitting will give better illumination.

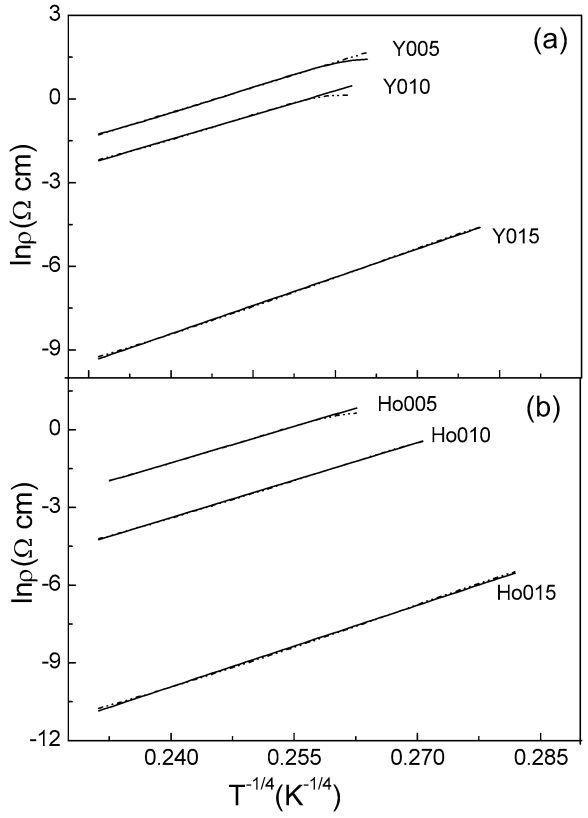

Fig. 3. The fitting plot of $\rho(T)$ curves of $La_{0.9-x}Y(Ho)_xTe_{0.1}MnO_3$ ($x = 0.05$, $x = 0.10$, and $x = 0.15$) according to the variable-range hopping model for the Y-doped (a) and Ho-doped (b).

3.3. Thermopower

Among various transport properties, thermopower is a simple and sensitive one for detecting scattering mechanism that dominates the electronic conduction because it is a zero current transport coefficient.

Fig. 4 shows the temperature dependence of thermopower $S(T)$ of both Y and Ho compounds in the temperature region of 5–350 K. Positive S in the whole measured region for

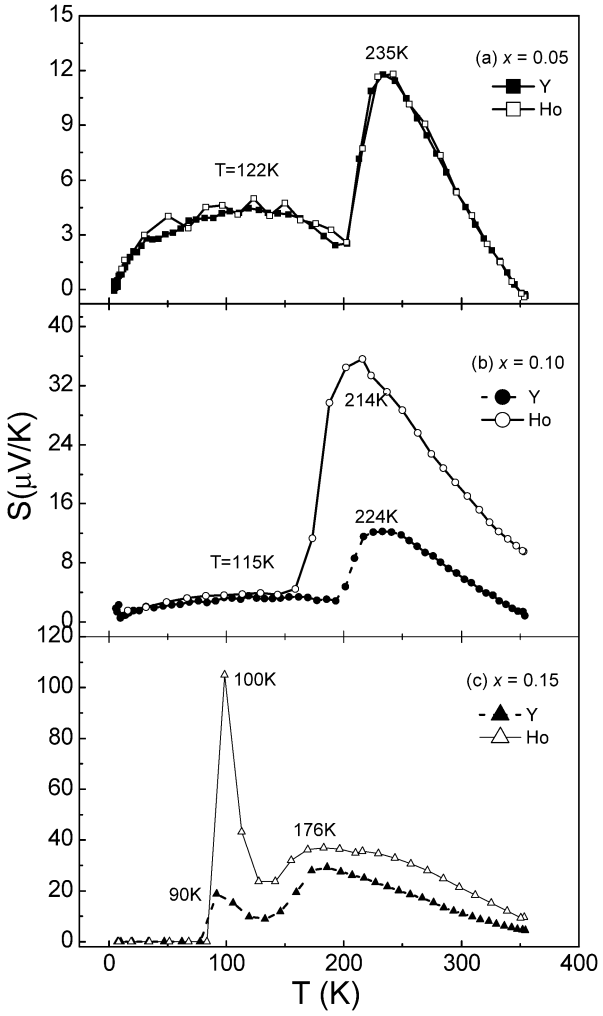

Fig. 4. The temperature dependence of thermopower S of $La_{0.9-x}Y(Ho)_xTe_{0.1}MnO_3$ with (a) $x = 0.05$, (b) $x = 0.10$, and (c) $x = 0.15$.

all samples is observed. Generally, S can indicate the kind of carrier in the compound. Therefore, it is very surprising to observe the positive S for $La_{0.9-x}A_xTe_{0.1}MnO_3$ (A = Y or Ho, $0.05 \leqslant x \leqslant 0.15$) samples that are regarded as electron-doped manganites. Recent many studies show S will become negative with increasing charge carrier density or temperature for the hole-doped manganites though it is expected that S is always positive for the hole-doped manganties [10,22]. That is to say, both electronlike and holelike bands can be present in these materials with the presence of Mn^{3+} and Mn^{4+}. Asmitsu et al. [23] have interpreted the change in sign observed in S, as a function of x and as a function of T, in terms of the change of electronic structure relating to the orbital degrees of freedom of the e_g carriers. The e_g band is built up with degenerate 3d orbitals ($d_{3z^2-r^2}$ and $d_{x^2-y^2}$), and is split into the upper and the lower band by an order of J_H. If the orbital degeneracy is not lifted in crystals for our studied samples, the average filling (n) of the lower e_g band in $La_{0.9-x}Y(Ho)_xTe_{0.1}MnO_3$ is $n = 0.9$ against the average full filling of $n = 1.5$. In this case, it is rather nature to suppose that the character of charge carriers is seen to be of hole type. By contrast, if the lower (up spin) band built up with the two orbitals is split further into two bands for some reason in our studied samples, then the lowest band is fulfilled when $n = 1$. In this case the actual average filling (n) is also smaller than the average full filling. Therefore, the carrier is always holelike in the studied samples. It is the reason why we can observe positive S for all our studied samples.

As the temperature decreases from 350 K, the S value for all samples increases and reaches a maximum at the temperature T_{S1}. The T_{S1} values are shown in Table 2. It can be seen that the T_{S1} is near T_{P1} but a little higher than its corresponding T_{P1} for all samples. The increase of S reflects the change of spin entropy due to the enhancement of spin polarization with decreasing the temperature. With decreasing the temperature further, a bump appears at $T_{S2} = 122$ and 115 K for the samples with $x = 0.05$ and $x = 0.10$, respectively, for both Y- and Ho-doped compounds. When x is increased to 0.15, the S exhibit a sharp peak at $T_{S2} = 90$ and 100 K for Y- and Ho-doped, respectively. It is worth pointing out that the T_{P2} value is not equal to its corresponding T_{S2} that suggests that the two temperatures have different origins. The bump or peak at T_{S2} is usually attributed to phonon drag effect, magon drag effect, and electron–magon scattering [11]. In addition, no any abnormality is observed at T^* for the Ho010 sample.

In order to gain further insight into the high-temperature conduction mechanism, we try to fit the thermopower S for all samples using the SP and VRH models.

At first, if the conduction in the high temperature proceeds via hopping of small polarons, then the thermopower is given by $S = \frac{k_B}{e}(\frac{E_0^S}{k_B T} + B)$, the experimental curves deviates from the fitting lines seriously for all samples (not shown here) which suggests that the conduction in the high temperature may be not dominated by the SP model.

Then we use the VRH model to fit the S data with the equation $S = K(T)^{1/2}$ and $K = \frac{k_B}{3e}\xi^2 T_0^{1/2}[\frac{d\ln N(\varepsilon)}{d\varepsilon}]$ [24], where ε is the energy measured from the Fermi level, ζ is a factor that determined the thickness of the energy layer within which the states are effective in conduction. T_0 is the factor appearing in the VRH formula $\rho \sim \exp(T_0/T)^{1/4}$. The results show that the VRH model is fully consistent with the S data for all samples as shown in Fig. 5(a) and (b).

Based on the discussion about fittings of the resistivity ρ and thermopower S, it is reasonable conclude that the electron conduction is governed by the VRH for all samples in the high temperature region. And with increasing the doping level, lattice distortion increases which results in the decrease of the localization length for electron. In addition, the magnetic disorder due to the competition of FM an AFM in the Ho-doping samples will result in the smaller of the localization length of Ho-doped comparing with that of Y-doped for the same composition.

3.4. Thermal conductivity

Measurements of the thermal conductivity give an attempt to study heat transport in the CMR compounds. The temperature dependence of thermal conductivity $\kappa(T)$ of $La_{0.9-x}A_xTe_{0.1}$-

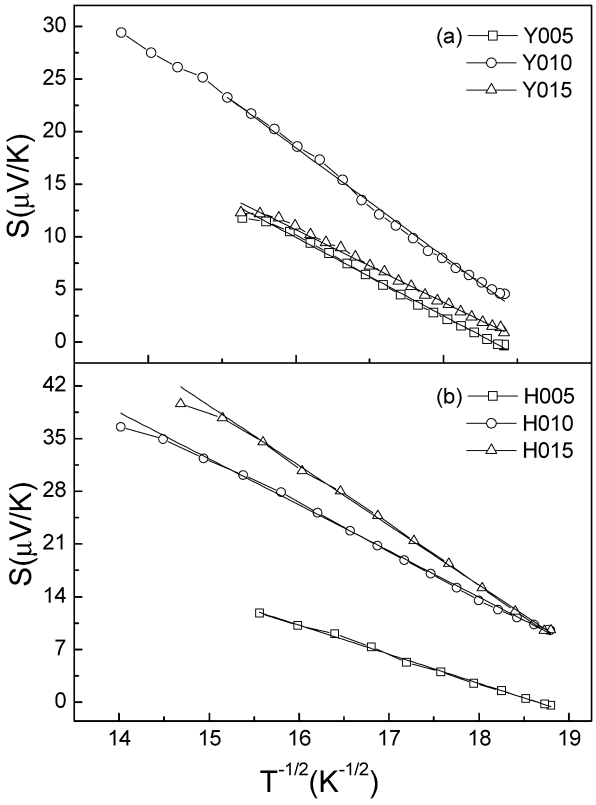

Fig. 5. The fitting plot of $S(T)$ curves of $La_{0.9-x}Y(Ho)_xTe_{0.1}MnO_3$ ($x = 0.05$, $x = 0.10$, and $x = 0.1$) according to the variable-range hopping model for the Y-doped (a) and Ho-doped (b).

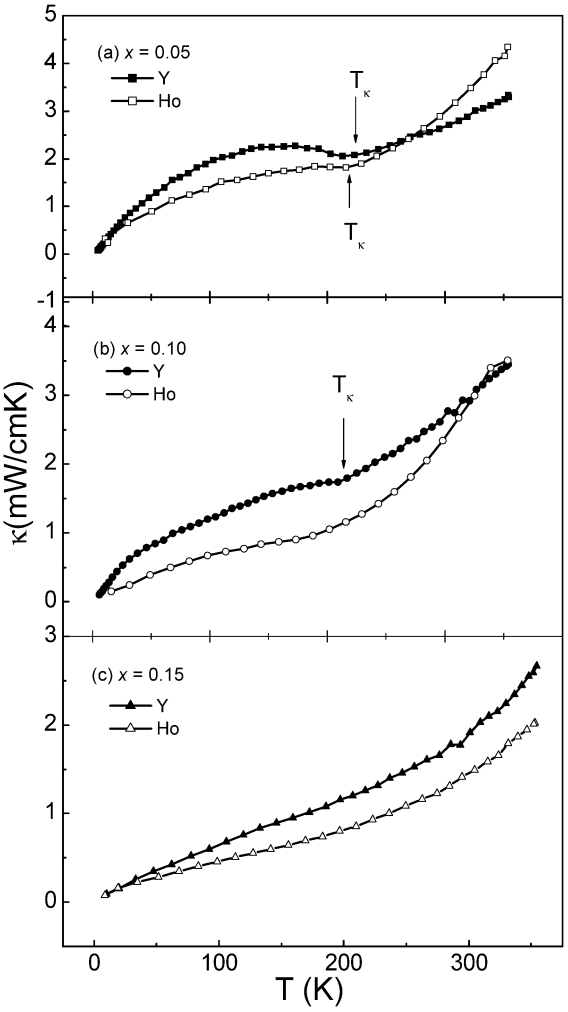

Fig. 6. The temperature dependence of thermal conductivity κ of $La_{0.9-x}Y(Ho)_xTe_{0.1}MnO_3$ with (a) $x = 0.05$, (b) $x = 0.10$, and (c) $x = 0.15$.

MnO_3 (A = Y or Ho, $0.05 \leqslant x \leqslant 0.15$) samples at zero field is shown in Fig. 6. It can be seen that the magnitude of κ lies in the range of 0–5 mW/(cm K), which is quite low for crystalline solids. Usually, the κ can be expressed by the sum of component (κ_{ph}) and mobile electron component (κ_e) as $\kappa = \kappa_{ph} + \kappa_e$. The κ_e value can be estimated from Wiedemann–Franz (W–F) law, which relates κ_e to ρ according to $\kappa_e = LT/\rho$, where L is Lorenz constant 2.45×10^{-8} W Ω/K^2, denotes the Lorenz number. Following this, our measured electrical resistivity data imply $\kappa_{el}/\kappa \sim 10^{-6}\%$ for the samples with $x = 0.05$, $\kappa_{el}/\kappa \sim 10^{-5}\%$ for the samples with $x = 0.10$, and $\kappa_{el}/\kappa \sim 10^{-3}\%$ for the samples with $x = 0.15$. It can be seen that the electronic contribution may be neglected for all samples and which indicates that the heat transport in our studied manganites is predominantly by the lattice vibration. In general, low value of κ is usually believed to be an indication of a high degree of disorder [25]. The local $Mn^{3+}O_6$ JT lattice distortion due to Mn^{3+} JT ions can scatter the phonon and gives rise to the decrease in κ. In our samples, the number of Mn^{3+} ions is fixed, therefore, the local $Mn^{3+}O_6$ JT lattice distortion is also fixed and it is constant for all samples. However, on the other hand, the lattice distortion due to the Y- or Ho-doping in La site, which hinders a strong increase in the mean free path of the phonon, which results in the decrease of κ for the same doping element with increasing the doping level. In addition, comparing with the same doping level for the Y- and Ho-doping level, it can be seen that κ for the Y-doping sample is larger than that for the Ho-doping one. In Ref. [26], the authors found that in the $La_{1-y}Sr_yMnO_3$ the thermal conductivity significantly decrease at $T < T_N$ upon transition from the FM conducting composition with $y = 0.48$ ($T_{FM} = 290$ K) to the AFM insulating composition with $y = 0.50$ ($T_{AFM} = 290$ K). And the author claimed that the AFM coupling would enhance phonon–phonon scattering and result in the decrease of thermal conductivity. Based on the above discussion, we may suggest that in our studied samples, the existence of AFM coupling between Ho and Mn ions, on the one hand, increases magnetic disorder and hence decreases the thermal conductivity, on the other hand, this coupling enhances the phonon–phonon scattering and results in the smaller thermal conductivity. Therefore, it is reasonable that the smaller of κ for the Ho-doping samples comparing with Y-doping results from the existence of AFM between Ho and Mn ions.

For the Y005, Ho005, and Y010 samples, κ can be divided into two regimes, that is, positive $d\kappa/dT$ in high and low temperature regions, and negative $d\kappa/dT$ well below T_κ (which is close T_{P1}). However, for the Y015, Ho010, and Ho015 samples, in the whole measured temperature only positive $d\kappa/dT$ can be observed. Similar phenomenon is also observed in the

hole-doped manganites [9] and the positive $d\kappa/dT$ is suggested be related to local anharmonic lattice distortions [9]. As to the origin of the negative $d\kappa/dT$ for the Y005, Ho005, and Y010 samples well below T_C, it is attributed the fact that JT distortions become delocalized along with the charge carriers and thereby reduces the phonon–phonon scattering. Therefore, it is reasonable to conclude that no same phenomenon will occur in the Y015, Ho010, and Ho015 samples as shown in Fig. 6. These results indicate that the enhancement of thermal conductivity below T_{P1} cannot be linked to the FM transition alone and is rather due to a transition from metal to insulator that suppresses significantly the amplitude of JT distortions reduces the phonon–phonon scattering and make the decrease of thermal conductivity.

4. Conclusion

In summary, we have investigated the electric resistivity, thermopower, and thermal conduction properties of the electron-doped manganites $La_{0.9-x}A_xTe_{0.1}MnO_3$ (A = Y or Ho, $0.05 \leqslant x \leqslant 0.15$). The electrical conduction at high temperatures has VRH behavior for all samples. The small thermal conduction data suggests that there exists a large JT distortion in the studied samples. Moreover, comparing with the Y-doped compounds, the Ho-doped ones have smaller the thermal conduction value. This result is discussed as the existence of antiferromagnetic (AFM) coupling between Ho and Mn ions in the Ho-doping samples. On the one hand, the magnetic disorder enhancement due to the competition of FM and AFM lower the thermal conductivity, on the other hand, the AFM coupling will reduce the phonon–phonon scattering.

Acknowledgements

This work was supported by the National Key Research under contract No. 001CB610604, and the National Nature Science Foundation of China under contract Nos. 10474100, 10374033, and the Fundamental Bureau of the Chinese Academy of Sciences.

References

[1] R. von Heklmolt, J. Wecker, B. Holzapfel, L. Schultz, K. Samwer, Phys. Rev. Lett. 71 (1993) 2331.
[2] A.P. Ramirez, J. Phys.: Condens. Matter 9 (1997) 8171.
[3] K. Chahara, T. Ohno, M. Kasai, Y. Kosono, Appl. Phys. Lett. 63 (1993) 1990.
[4] C. Zener, Phys. Rev. 82 (1951) 403.
[5] A.J. Mills, P.B. Littlewood, B.I. Shraiman, Phys. Rev. Lett. 74 (1995) 5144.
[6] P. Mandal, S. Das, Phys. Rev. B 56 (1997) 15073.
[7] G.T. Tan, S.Y. Dai, P. Duan, Y.L. Zhou, H.B. Lu, Z.H. Chen, J. Appl. Phys. 93 (2003) 5480.
[8] S. Roy, N. Ali, J. Appl. Phys. 89 (2001) 7425.
[9] D.W. Visser, A.P. Ramirez, M.A. Subramanian, Phys. Rev. Lett. 78 (1997) 3947.
[10] V.H. Crespi, L. Lu, Y.X. Jia, K. Khazeni, A. Zettl, M.L. Cohen, Phys. Rev. B 53 (1996) 14303.
[11] B.X. Chen, A.G. Rojo, C. Uher, Phys. Rev. B 55 (1997) 15471.
[12] J.L. Cohn, J.J. Neumeier, C.P. Popoviciu, K.L. McClellan, Th. Leventouri, Phys. Rev. B 56 (1997) R8495.
[13] S.L. Ye, W.H. Song, J.M. Dai, S.G. Wang, K.Y. Wang, C.L. Yuan, Y.P. Sun, J. Appl. Phys. 88 (2000) 5915.
[14] S.L. Ye, W.H. Song, J.M. Dai, K.Y. Wang, S.G. Wang, J.J. Du, Y.P. Sun, J. Fang, J.L. Chen, B.J. Gao, J. Appl. Phys. 90 (2000) 2943.
[15] M. Itoh, T. Shimura, J.D. Yu, T. Hayashi, Y. Inaguma, Phys. Rev. B 52 (1995) 12522.
[16] X.L. Wang, S.L. Kennedy, H.K. Liu, S.X. Dou, J. Appl. Phys. 83 (1998) 7177.
[17] R.S. Freitas, L. Ghivelder, F. Damay, F. Dias, L.F. Cohen, Phys. Rev. B 64 (2001) 144404;
S.M. Yusuf, K.R. Chakraborty, S.K. Paranjpe, R. Ganguly, P.K. Mishra, J.V. Yakhmi, V.C. Sahni, Phys. Rev. B 68 (2003) 104421.
[18] G.H. Zheng, Y.P. Sun, et al., unpublished.
[19] J. Hemberger, S. Lobina, H.-A. Krug von Nidda, N. Tristan, V.Y. Ivanov, A.A. Mukhin, A.M. Balbashov, A. Loidl, Phys. Rev. B 70 (2004) 024414.
[20] G.J. Snyder, C.H. Booth, F. Bridges, R. Hiskes, S. DiCarolis, M.R. Beasley, T.H. Geballe, Phys. Rev. B 55 (1997) 6453.
[21] G.J. Snyder, R. Hiskes, S. DiCarolis, M.R. Beasley, T.H. Geballe, Phys. Rev. B 53 (1998) 14103.
[22] P. Mandal, Phys. Rev. B 61 (2000) 14675.
[23] A. Asamitsu, Y. Moritomo, Y. Tokura, Phys. Rev. B 53 (1996) R2952.
[24] N.F. Mott, in: J. Treusch (Ed.), Festkörperprobleme, vol. 19, Vieweg, Braunschweig, 1979, p. 341.
[25] J.L. Cohn, J. Supercond.: Inorp. Novel Magnetism 12 (1999) 281.
[26] M. Ikebe, H. Fujishiro, S. Kanoh, T. Mikami, Phys. Status Solidi B 225 (2001) 135.